Computation of the mitochondrial age distribution along the axon length

Ivan A. Kuznetsov[(a), (b)] and Andrey V. Kuznetsov[(c)]

[(a)] Perelman School of Medicine, University of Pennsylvania, Philadelphia, PA 19104, USA

[(b)] Department of Bioengineering, University of Pennsylvania, Philadelphia, PA 19104, USA

[(c)] Department of Mechanical and Aerospace Engineering, North Carolina State University, Raleigh, NC 27695-7910, USA; e-mail: avkuznet@ncsu.edu

Abstract

Here, we describe a compartmental model of mitochondrial transport in axons, which we apply to compute mitochondrial age at different distances from the soma. The model predicts that the average mitochondrial age at the tip of an axon with a length of 1 cm is approximately 20 hours. The mitochondria are youngest closest to the soma and their age scales approximately linearly with distance from the soma. To the best of the authors' knowledge, this is the first attempt to predict the spatial distribution of mitochondrial age within an axon. A sensitivity study of the mean age of mitochondria to various model parameters is also presented.

Keywords: neurons; axonal transport; organelles; mean age; mathematical modeling

1. Introduction

Mitochondria generate easily usable chemical power for cells. In addition to their direct involvement in cellular respiration, they are also involved in apoptosis, calcium buffering, and many other important biological functions [1,2]. Abnormalities in mitochondrial transport occur in many neurological disorders [3]. Recent research implicates α-synuclein-induced disruptions of mitochondrial trafficking in the development of Parkinson's disease (PD) [4,5]. Since packed mitochondria membrane fragments are one of the components found in Lewy bodies [5], investigating the transport of mitochondria is important for understanding the fundamentals of PD, for example in regards to possible energy deficits in dopaminergic neurons due to disruptions in mitochondrial axonal transport [6].

There are three pools of mitochondria in axons: anterogradely transported, retrogradely transported, and stationary [7]. Understanding how old are mitochondria in these pools, and also how their age depends on the distance from the soma is important to understand how mitochondria are renewed in the axon, and also what can go wrong with mitochondrial transport in various diseases. Estimating the age of mitochondria may be important, for example, in evaluating the possible role of oxidative damage in the development of various neurodegenerative diseases [8].

Renewal of mitochondrial proteins involves mitochondrial fusion and fission [9]. Fusion of old and new mitochondria leads to an exchange of old and new soluble and membrane-bound components, such as mitochondrial proteins [10,11]. Mitochondrial fission is believed to lead to separating mutated copies of the mitochondrial genome into a separate mitochondrion, which is then recycled by the autophagosome [12,13]. Fission also serves as a mechanism preventing mitochondria from becoming excessively long, so longer mitochondria are more likely to enter fission than shorter ones [14]. If fission events are unopposed, they can lead to complete fragmentation of the mitochondrial network [15]. Mitochondrial fusion accelerates mitochondrial fission, which is necessary to maintain a constant average length of mitochondria. Fission is important for autophagy, the mechanism of mitochondria removal [12].

Mitochondria are moved anterogradely by kinesin (in particular, by kinesin-1) motors and retrogradely by cytoplasmic dynein [16]. The motion of individual mitochondria is not continuous but rather interrupted by frequent pauses. Mitochondria move with an average velocity of 0.4-0.8 μm/s [17].

For investigating mitochondria mean age distribution in various compartments surrounding demand sites, ref. [18] used a photoconvertible construct, termed MitoTimer, that switches from green to red fluorescence over a period of hours due to slow oxidation as it ages (red corresponds to older mitochondria and green corresponds to younger mitochondria). MitoTimer exhibits green fluorescence for the first 8 hours. After 24 hours it shows a mixture of green and red fluorescence (producing a yellow color). After 48-72 hours MitoTimer exhibits red fluorescence [18-21]. Experiments reported in [18] that mitochondria residing in compartments surrounding the more distal demand sites are older than those residing in compartments surrounding the more proximal demand sites. The ratio of red/green fluorescence depends on the rate of mitochondria synthesis in the soma, the rate of mitochondrial transport in the axon, the rates of fusion and fission (which equilibrate the MitoTimer protein content in mitochondria and mitochondria age), and autophagy.

A computational study [11] investigated mitochondria health, which is a proxy for mitochondrial membrane potential. An initial population of 150 unfused mitochondria was simulated. Recent research [22] developed models for two maintenance models of mitochondria, one that assumed the exchange of mitochondrial proteins between moving and stationary mitochondria due to mitochondrial fusion and fission, and the other that assumed occasional replacement of stationary mitochondria with new ones, arriving from the soma.

2. Materials and models

2.1. Governing equations

The model developed in this paper accounts for stationary and anterogradely and retrogradely moving mitochondria. We simulated a terminal with N high energy demand sites (hereafter demand sites) that contain stationary mitochondria (Fig. 1). The model developed in this research accounts for N resident and $2N$ transiting (anterograde and retrograde) kinetic states and contains $3N$ ODEs (we used N=10 in this research).

We used a multi-compartment model [23-25] to formulate equations expressing the conservation of the total length of mitochondria in the compartments. We used a similar compartmental approach to simulate the transport of dense core vesicles in *Drosophila* motoneurons [26,27]. We numbered the demand sites in the axon terminal from the most proximal #1 to the most distal #N (Fig. 1). The demand sites have three compartments (representing resident, transiting-anterograde, and transiting-retrograde pools of mitochondria), see Fig. 2.

Since the length of an axon is much greater than its width, we used the total length of mitochondria in the kinetic state per unit axon length, measured in (μm of mitochondria)/μm. The total length of mitochondria is defined as the sum of the lengths of all mitochondria residing in the same kinetic state (stationary, anterograde, or retrograde) in the same compartment. The total length of mitochondria in the compartment for a particular kinetic state (Fig. 2) is the conserved quantity. The dependent variables utilized in the model are summarized in Table 1.

Table 1. Dependent variables in the model of mitochondrial transport and accumulation in the axon.

Symbol	Definition	Units
l_i^s	Total length of stationary mitochondria per unit length of the axon in the compartment by the *i*th demand site	(μm of mitochondria)/μm
l_i^a	Total length of anterogradely moving mitochondria per unit length of the axon in the compartment by the *i*th demand site	(μm of mitochondria)/μm
l_i^r	Total length of retrogradely moving mitochondria per unit length of the axon in the compartment by the *i*th demand site	(μm of mitochondria)/μm
$j_{a\to b}$	Flux of mitochondria length from state (compartment) *a* to state (compartment) *b*	(μm of mitochondria) s^{-1}

First, the conservation of the total mitochondria length in the compartment around the most proximal demand site (# 1) is formulated. Stating this for the stationary pool of mitochondria gives the following equation (Fig. 2):

$$L_1 \frac{dl_1^s}{dt} = p_s \left(j_{soma\to 1} + j_{2\to 1} \right) - L_1 k_w l_1^s , \tag{1}$$

where L_1 is the length of an axonal compartment around the most proximal mitochondria demand site and *t* is the time. We assumed that the axonal length L_{ax} is split into *N* compartments of equal length, for example, $L_1 = L_{ax} / N$.

The conservation of mitochondria length in the anterograde pool of mitochondria around demand site 1 gives the following equation (Fig. 2):

$$L_1 \frac{dl_1^a}{dt} = j_{soma\to 1} - p_s j_{soma\to 1} - j_{1\to 2} + \varepsilon L_1 k_w l_1^s . \tag{2}$$

Unlike [22], we assumed that mitochondria that reenter the motile state are not split evenly between the anterograde and retrograde components. Rather, the portion of mitochondria that reenter the anterograde component is given by ε and the portion of mitochondria that reenter the retrograde component is given by $(1-\varepsilon)$ (see Fig. 2 and Table 2).

The conservation of mitochondria length in the retrograde pool of mitochondria around the most proximal demand site gives the following equation (Fig. 2):

$$L_1 \frac{dl_1^r}{dt} = j_{2\to 1} - p_s j_{2\to 1} - j_{1\to soma} + (1-\varepsilon) L_1 k_w l_1^s . \tag{3}$$

Next, the conservation of mitochondria length in the compartment around the *i*th demand site (*i*=2,..,*N*-1) is formulated. The conservation of mitochondria length in the stationary pool around the *i*th demand site gives the following equation (Fig. 2):

$$L_i \frac{dl_i^s}{dt} = p_s \left(j_{i-1\to i} + j_{i+1\to i} \right) - L_i k_w l_i^s . \tag{4}$$

The conservation of mitochondria length in the anterograde pool in the *i*th demand site gives the following equation (Fig. 2):

$$L_i \frac{dl_i^a}{dt} = j_{i-1\to i} - p_s j_{i-1\to i} - j_{i\to i+1} + \varepsilon L_i k_w l_i^s . \tag{5}$$

The conservation of mitochondria length in the retrograde pool in the *i*th demand site gives the following equation (Fig. 2):

$$L_i \frac{dl_i^r}{dt} = j_{i+1\to i} - p_s j_{i+1\to i} - j_{i\to i-1} + (1-\varepsilon) L_i k_w l_i^s . \tag{6}$$

Finally, the conservation of mitochondria length in the compartment around the most distal demand site (# *N*) is formulated. The conservation of mitochondria length in the stationary pool gives the following equation (Fig. 2):

$$L_N \frac{dl_N^s}{dt} = p_s \left(j_{N-1\to N} + j_{N\to 3N} \right) - L_N k_w l_N^s . \tag{7}$$

The conservation of mitochondria length in the anterograde pool gives the following equation (Fig. 2):

$$L_N \frac{dl_N^a}{dt} = j_{N-1\to N} - p_s j_{N-1\to N} - j_{N\to N-1} + \varepsilon L_N k_w l_N^s . \tag{8}$$

The conservation of mitochondria length in the retrograde pool gives the following equation (Fig. 2):

$$L_N \frac{dl_N^r}{dt} = j_{N\to 3N} - p_s j_{N\to 3N} - j_{N\to N-1} + (1-\varepsilon) L_N k_w l_N^s . \tag{9}$$

Eqs. (1)-(9) must be supplemented by the following equations for the mitochondria fluxes between the demand sites. $j_{soma\to 1}$ is an input model parameter; equations for other anterograde fluxes (Fig. 2) are

$$j_{1\to 2} = v_a l_1^a , \tag{10}$$

…

$$j_{i-1\to i} = v_a l_{i-1}^a , \tag{11}$$

$$j_{i\to i+1} = v_a l_i^a , \tag{12}$$

…

$$j_{N-1\to N} = v_a l_{N-1}^a , \tag{13}$$

$$j_{N\to 3N} = v_a l_N^a . \tag{14}$$

Equations for retrograde fluxes (Fig. 2) are

$$j_{N\to N-1} = v_r l_N^r , \tag{15}$$

…

$$j_{i+1\to i} = v_r l_{i+1}^r , \tag{16}$$

$$j_{i\to i-1} = v_r l_i^r , \tag{17}$$

…

$$j_{2\to 1} = v_r l_2^r , \tag{18}$$

$$j_{1\to soma} = v_r l_1^r . \tag{19}$$

Since we seek the steady-state solution (which is of physical significance), the initial condition does not matter. We solved Eqs. (1)-(9) with zero initial conditions in all compartments and proceeded until the solution reached steady-state.

Table 2. Parameters characterizing mitochondrial transport and accumulation in the axon.

Symbol	Definition	Units	Value or range	Reference(s)	Value used in computations
v_a	Average velocity of anterogradely moving mitochondria	$\mu m\, s^{-1}$	0.5	[22]	0.5
v_r	Average velocity of retrogradely moving mitochondria	$\mu m\, s^{-1}$	0.5	[22]	0.5
$j_{soma \to 1}$	Rate of mitochondria production in the soma	mitochondria s^{-1}	0.0375	[22]	0.0375 [a]
L_{ax}	Length of the axon	μm	10^4 - 10^5	[22]	10^4
k_w	Kinetic constant characterizing the rate of mitochondria reentry into motile states (anterograde and retrograde)	s^{-1}	$2\times10^{-4} - 2\times10^{-3}$ [b]	[22]	2×10^{-4}
ε	Portion of mitochondria leaving the stationary state that join the anterograde pool; $(1-\varepsilon)$ join the retrograde pool		0.5	[22]	0.5
f_s	Fraction of stationary mitochondria		0.5-0.6	[22]	0.5
p_s	Probability that a motile mitochondrion would transition to a stationary state at a demand site		0.4-0.5	[22]	0.4
N	Number of demand sites in the axon		5-100 [c]	[22]	10

[a] We estimated $j_{soma \to 1}$ using the formula suggested in [22], $Mv/(2L)$, where M is the number of mitochondria in the axon, and v is the average velocity of mitochondria motion in the axon. We used 1,500 mitochondria for M, 0.5 μm/s for v, and 1 cm for L.

[b] We used Eq. (4) from ref. [22], $f_s = \frac{Nvp_s}{L_{ax}k_w + Nvp_s}$. By solving this equation for k_w using values given in Table 2 (for N we used the range 10-100), we obtained that k_w is in the range $2\times10^{-4} - 2\times10^{-3}\ \mathrm{s}^{-1}$.

[c] $p_s = \frac{N_s}{2N}$, where N_s is an average number of stops that a mitochondrion makes during a back and forth journey in the axon [22].

[d] Number of demand sites in a real axon can be much larger than that.

2.2. Model of mean age of mitochondria in the demand sites

To compute the age distributions of mitochondria in the stationary and moving states in the compartments surrounding the demand sites, the method described by [28,29] was utilized. Eqs. (1)-(9) were restated as the following matrix equation:

$$\frac{d}{dt}\mathbf{C}^*(t) = \mathrm{B}\left(\mathbf{C}^*(t),t\right)\mathbf{C}^*(t) + \mathbf{u}(t). \tag{20}$$

In Eq. (20) $\mathbf{C}^*$ is the state vector, which is defined by its components:

$$C_1^* = l_1L_1,\ldots,C_N^* = l_NL_N, C_{N+1}^* = l_1^aL_1,\ldots,C_{2N-1}^* = l_{N-1}^aL_{N-1}, C_{2N}^* = l_N^mL_N, C_{2N+1}^* = l_1^rL_1, C_{3N-1}^* = l_{N-1}^rL_{N-1}, \tag{21}$$

where

$$\hat{l}_1 = l_1,\ldots,\hat{l}_N = l_N, \hat{l}_{N+1} = l_1^a,\ldots,\hat{l}_{2N-1} = l_{N-1}^a, \hat{l}_{2N} = l_N^m, \hat{l}_{2N+1} = l_1^r, \hat{l}_{3N} = l_N^r. \tag{22}$$

The total length of mitochondria in stationary states is represented by the first N components of the state vector, the total length of mitochondria in anterograde states is represented by the next N components (N+1,…,2N), and the total length of mitochondria in retrograde states is represented by the last N components (2N+1,…,3N), see Fig. 2. Vector $\mathbf{u}(t)$ is defined below by Eqs. (45) and (46).

In our model, matrix B(3N,3N) is as follows. We accounted for the internal mitochondria fluxes between compartments, the external mitochondria flux entering the terminal from the axon, and the mitochondria flux leaving the terminal to move back to the axon (Fig. 2). Equations for the

following elements of matrix B were obtained by analyzing mitochondria fluxes to and from the compartments surrounding the most proximal demand site:

$$b_{N+1,1} = \varepsilon L_1 k_w l_1^s / \left(L_1 l_1^a \right), \tag{23}$$

$$b_{1,N+1} = p_s j_{soma \to 1} / \left(L_1 l_1^s \right), \tag{24}$$

$$b_{2N+1,1} = \left(1-\varepsilon\right) L_1 k_w l_1^s / \left(L_1 l_1^r \right), \tag{25}$$

$$b_{1,2N+1} = p_s j_{2 \to 1} / \left(L_1 l_1^s \right), \tag{26}$$

$$b_{N+2,N+1} = j_{1 \to 2} / \left(L_2 l_2^a \right), \tag{27}$$

$$b_{2N+1,2N+2} = j_{2 \to 1} / \left(L_1 l_1^r \right), \tag{28}$$

$$b_{2N+1,2N+1} = -j_{1 \to soma} / \left(L_1 l_1^r \right), \tag{29}$$

The analysis of mitochondria fluxes to and from the compartments surrounding demand site i (i=2,…,N-1) gives equations for the following elements of matrix B:

$$b_{N+i,i} = \varepsilon L_i k_w l_i^s / \left(L_i l_i^a \right), \tag{30}$$

$$b_{i,N+i} = p_s j_{i-1 \to i} / \left(L_i l_i^s \right), \tag{31}$$

$$b_{2N+i,i} = \left(1-\varepsilon\right) L_i k_w l_i^s / \left(L_i l_i^r \right), \tag{32}$$

$$b_{i,2N+i} = p_s j_{i+1 \to i} / \left(L_i l_i^s \right), \tag{33}$$

$$b_{N+i,N+i-1} = j_{i-1 \to i} / \left(L_i l_i^a \right), \tag{34}$$

$$b_{N+i+1,N+i} = j_{i \to i+1} / \left(L_{i+1} l_{i+1}^a \right), \tag{35}$$

$$b_{2N+i-1,2N+i} = j_{i \to i-1} / \left(L_{i-1} l_{i-1}^r \right), \tag{36}$$

$$b_{2N+i,2N+i+1} = j_{i+1 \to i} / \left(L_i l_i^r \right), \tag{37}$$

By analyzing mitochondria fluxes to and from the compartments surrounding the most distal demand site, equations for the following elements of matrix B were obtained:

$$b_{2N,N} = \varepsilon L_N k_w l_N^s / \left(L_N l_N^a \right), \tag{38}$$

$$b_{N,2N} = p_s j_{N-1\to N} / \left(L_N l_N^s \right), \tag{39}$$

$$b_{2N,2N-1} = j_{N-1\to N} / \left(L_N l_N^a \right), \tag{40}$$

$$b_{3N,2N} = j_{N\to 3N} / \left(L_N l_N^r \right), \tag{41}$$

$$b_{3N,N} = \left(1-\varepsilon\right) L_N k_w l_N^s / \left(L_N l_N^r \right), \tag{42}$$

$$b_{N,3N} = p_s j_{N\to 3N} / \left(L_N l_N^s \right), \tag{43}$$

$$b_{3N-1,3N} = j_{N\to N-1} / \left(L_{N-1} l_{N-1}^r \right). \tag{44}$$

All other elements of matrix B, except for those given by Eqs. (23)-(44), are equal to zero.

The anterograde flux from the axon to the compartment with anterograde mitochondria by the most proximal demand site, $j_{soma\to 1}$, is the only flux entering the terminal. Our model assumes that all mitochondria that leave the terminal (their flux is $j_{soma\to 1}$) return to the soma for degradation, and none of them reenter the terminal. We also assumed that mitochondria that enter the terminal (their flux is $j_{soma\to 1}$) are all newly synthesized in the soma, and their age at the time of entry is equal to zero. This means that our model does not account for the time it takes mitochondria to travel from the soma to the terminal. The mitochondrial age calculated here should be understood as the time since mitochondria entered the terminal.

The following equation yields the N+1 element of vector **u**:

$$u_{N+1} = j_{soma\to 1}. \tag{45}$$

Because no other external fluxes enter the terminal,

$$u_i = 0 \quad (i=1,\ldots,N,N+2,\ldots,3N-1). \tag{46}$$

The state transition matrix, Φ, may be determined by solving the following matrix equation [28]:

$$\frac{d}{dt}\Phi\left(t,t_0\right) = \mathrm{B}\left(\mathbf{N}^*\left(t\right),t\right)\Phi\left(t,t_0\right). \tag{47}$$

The initial condition for Eq. (47) is

$$\Phi\left(t_0,t_0\right) = \mathrm{I}. \tag{48}$$

In Eq. (48) symbol I denotes an identity matrix.

We assumed that all mitochondria that enter the terminal are new. The age density of mitochondria entering the terminal after $t=0$ can then be determined from the following equation:

$$\mathbf{p}(c,t)=1_{[0,t-t_0)}(c)\Phi(t,t-c)\mathbf{u}(t-c), \tag{49}$$

where $1_{[0,t-t_0)}$ is the indicator function, which equals 1 if $0 \le c < t-t_0$ and equals 0 otherwise. The age density of mitochondria is the ratio of the total length of mitochondria in the compartment which have an age between *T* and *T*+*dT* over the duration of this interval *dT*. An integral of the age density of mitochondria over any time period with respect to time gives the length of mitochondria having an age within that time range.

The mean age of mitochondria in demand sites is [30]:

$$\overline{c}_i(t)=\frac{\int_0^\infty cp_i(c,t)dc}{\int_0^\infty p_i(c,t)dc} \qquad (i=1,\ldots,3N). \tag{50}$$

$\overline{c}_i(t)$ (i=1,…,3N) may be found by solving the following mean age system [28,30]:

$$\frac{d}{dt}\overline{\mathbf{c}}(t)=\mathbf{g}\left(\mathbf{N}^*(t),t\right). \tag{51}$$

The initial condition for Eq. (51) is

$$\overline{\mathbf{c}}(0)=0, \tag{52}$$

where $\overline{\mathbf{c}}=\left(\overline{c}_1,\ldots,\overline{c}_{3N}\right)$. Vector **g** is defined as follows:

$$g_i(t)=1+\frac{\sum_{j=1}^{3N}\left(\overline{c}_j(t)-\overline{c}_i(t)\right)b_{i,j}(t)N_j(t)-\overline{c}_i(t)u_i}{N_i(t)} \qquad (i=1,\ldots,3N). \tag{53}$$

The following vectors were then defined to represent the mean age of mitochondria in the stationary, anterograde, and retrograde states in the demand sites, respectively:

$$\mathbf{a}_s=\left(\overline{c}_1,\ldots,\overline{c}_N\right),\ \mathbf{a}_a=\left(\overline{c}_{N+1},\ldots,\overline{c}_{2N}\right),\ \mathbf{a}_r=\left(\overline{c}_{2N+1},\ldots,\overline{c}_{3N}\right). \tag{54}$$

The arrays $\mathbf{a}_s$, $\mathbf{a}_a$, and $\mathbf{a}_r$ are one-dimensional of size *N*.

Numerical solutions were obtained utilizing Matlab's solver, ODE45 (Matlab R2019a, MathWorks, Natick, MA, USA). The error tolerance parameters, RelTol and AbsTol, were set to 10^{-6} and 10^{-8}, respectively. We checked that lowering RelTol and AbsTol did not influence the solutions.

3. Results

3.1. Estimation of the average age of mitochondria in the most distal demand site

According to Fig. 4C in [18], at some point in time the green/red fluorescence ratio linearly decreases with an increase of the distance from the nucleus as:

$$y = -0.5863x + 2303.5\,, \tag{55}$$

where x is in μm and y is in arbitrary units. From Eq. (55) it follows that

$$\frac{dy}{dx} = -0.5863\,. \tag{56}$$

In [18] MitoTimer production was induced by exposure to doxycycline. Green fluorescence starts approximately 5 h after doxycycline induction, at that point in time red fluorescence is equal to zero (Fig. 2A in [18]). According to Fig. 2A in [18], the red/green fluorescence ratio, which is reciprocal of y, is approximately given by

$$z = \frac{1.5}{55} t_{mit}\,, \tag{57}$$

where t_{mit} must be given in hours ($t_{mit} = 0$ corresponds to approximately 5 h after doxycycline induction, the time when green fluorescence starts while red fluorescence is equal to zero, see Fig. 1C from [18]).

At x=0 we assumed that all mitochondria are newly synthesized and therefore their age is zero. For the estimate of the mitochondrial age at the axon terminal, we assumed a direct relation between the age of a mitochondrion, t_{mit}, and its distance from the soma (this assumption is supported by [31]):

$$t_{mit} = \lambda x\,. \tag{58}$$

Comparing Eqs. (56), (57), and (58) follows that

$$\frac{dy}{dx} = \frac{d}{dx}\left(\frac{1}{z}\right) = -\frac{55}{1.5}\frac{1}{\lambda x^2} = -0.5863 \,. \tag{59}$$

We used Eq. (59) at $x = 200$ μm (one-third of the range displayed in Fig. 4C of [18]) and solved this equation for λ. The result is

$$\lambda = 1.56 \times 10^{-3} \text{ h μm}^{-1}. \tag{60}$$

Calculating the age of mitochondria at the axon tip (at $x = L_{ax}$) leads to

$$t_{mit,x=L} = \lambda L_{ax} = 15.6 \text{ h}. \tag{61}$$

This is consistent with the expected half-life of mitochondrial proteins (days or weeks) [9]. It is interesting that data obtained in [32] using Timer fluorescent protein support rapid turnover of mitochondria in axon terminals and suggest that the residence time of the protein in the synapse is approximately 3 hours. Ref. [33] reported that complete turnover of mitochondria in axon terminals of zebrafish neurons occurs within 24 hours.

3.2. Total length of various populations of mitochondria per unit length of the axon and mean age of mitochondria in various demand sites

The total length of stationary mitochondria at steady-state is the largest, followed by the total length of anterogradely and then retrogradely moving mitochondria. . The largest concentration of stationary mitochondria is at the proximal demand site, then it gradually decreases and reaches a minimum at demand site # 8; it then slightly increases due to the accumulation of mitochondria as they turn around at the tip of the axon (Fig. 3). Computations with $k_w = 2 \times 10^{-4}$ s^{-1} (Table 2) yield the mean age of stationary mitochondria in demand site # 10 (the most distal demand site) to be approximately 21.8 h (Fig. 3), which is consistent with the estimate given by Eq. (61). It is known that older mitochondria may have impaired function due to accumulated oxidative damage [34]. However, since the age of mitochondria at the tip of an axon with a length of 1 cm is only 20 hours, oxidative damage is unlikely to be a contributing factor in mitochondrial disorders in such short axons.

The mean ages of stationary, anterograde, and retrograde mitochondria increase from the proximal to more distal demand sites. The mean age of retrograde mitochondria is slightly (approximately 20%) less than the mean age of stationary mitochondria in the same demand site. The mean ages of anterograde and stationary mitochondria are close to each other (Fig. 4). This is

in agreement with results reported in [18,31], which found that the age of mitochondria increased approximately linearly with distance from the soma, and found no sharp age difference between motile and stationary pools of mitochondria.

The mean age of stationary mitochondria of 21.8 h in the most distal demand site is severalfold greater than the time it takes for the mitochondria to travel from the soma to the most distal demand site without stops:

$$L_{ax} / v = \left(10^4 \mu\text{m}\right) / \left(0.5 \mu\text{m} / s\right) = 2 \times 10^4 \text{ s} = 5.56 \text{h} << 21.8 \text{h} . \tag{62}$$

3.3. Investigating sensitivity of the mean age of mitochondria in demand sites on parameters k_w, p_s, and ε

To investigate the sensitivity of the solution to the model parameters whose values are hardest to estimate, k_w p_s, and ε, we calculated the local sensitivity coefficients, which are first-order partial derivatives of the observables with respect to model parameters [35-38]. For example, the sensitivity coefficient of the mean age of resident mitochondria in demand sites to parameter k_w at steady-state (ss) can be calculated as follows:

$$\frac{\partial a_{i,ss}}{\partial k_w} \approx \left. \frac{a_{i,ss}\left(k_w + \Delta k_w\right) - a_{i,ss}\left(k_w\right)}{\Delta k_w} \right|_{\text{other parmeters kept constant}} \qquad (i=1,\ldots,N), \tag{63}$$

where $\Delta k_w = 10^{-3} k_w$ (the accuracy was tested by using various step sizes).

The sensitivity coefficients were non-dimensionalized by introducing relative sensitivity coefficients [36,39], defined as (for example):

$$S_{k_w}^{\bar{a}_{i,ss}} = \frac{k_w}{a_{i,ss}} \frac{\partial a_{i,ss}}{\partial k_w} \qquad (i=1,\ldots,N). \tag{64}$$

The dimensionless sensitivity of the mean age of mitochondria to k_w is negative in all demand sites (Fig. 5). This means that the increase of k_w leads to a decrease of the mean age of mitochondria in all demand sites. The sensitivity slightly increases toward more distal demand sites.

The dimensionless sensitivity of the mean age of mitochondria to p_s is positive in all demand sites (Fig. 6). This means that the increase of p_s leads to an increase in the mean age of

mitochondria in all demand sites. The sensitivity slightly increases toward more distal demand sites.

The dimensionless sensitivity of the mean age of stationary and retrograde mitochondria to ε is negative in the proximal demand sites and positive in the distal demand sites. This means that the increase of ε leads to a decrease of the mean age of stationary and retrograde mitochondria in proximal demand sites and to an increase of the mean age of stationary and retrograde mitochondria in the more distal demand sites. The dimensionless sensitivity of the mean age of anterograde mitochondria to ε is slightly positive even in the most proximal demand site and then increases toward more distal demand sites (Fig. 7).

4. Discussion, limitations of the model and future directions

The model gives quantitative predictions for the distribution of mitochondrial mean age throughout the axon length that can be tested experimentally, indicating that the model has predictive value. The model thus suggests further experiments that could be used to confirm the model's predictions, especially with respect to mitochondrial age distribution in various demand sites.

The model predicts that the mean age of stationary mitochondria in the most distal demand site is approximately 21.8 h. This is severalfold greater than the time it takes for mitochondria to travel without stopping from the soma to the farthest demand location. To quantify the dependence of the solutions on model parameters, we employed analysis of the dimensionless sensitivity of the mean age of mitochondria at demand sites.

Future development of the model should address the following points. Mitochondria that return to the soma from the axon are usually not destroyed, but rather fuse with a resident somatic pool of mitochondria [9]. Therefore, our assumption that mitochondria have zero age at the entrance to the axon is a simplifying one. Future model development should address this issue.

Acknowledgment

IAK acknowledges the fellowship support of the Paul and Daisy Soros Fellowship for New Americans and the NIH/National Institutes of Mental Health (NIMH) Ruth L. Kirchstein NRSA (F30 MH122076-01). AVK acknowledges the support of the National Science Foundation (award

CBET-2042834) and the Alexander von Humboldt Foundation through the Humboldt Research Award.

References

1. Fan T, Xia L, Han Y. Mitochondrion and apoptosis. *Acta Biochimica Et Biophysica Sinica* 2001; **33**(1): 7-12.
2. Picard M, McEwen BS. Psychological stress and mitochondria: A systematic review. *Psychosomatic Medicine* 2018; **80**(2): 141-153.
3. Zheng Y, Zhang X, Chen Z. Mitochondrial transport serves as a mitochondrial quality control strategy in axons: Implications for central nervous system disorders. *Cns Neuroscience & Therapeutics* 2019; **25**(7): 876-886.
4. Clague MJ, Rochin L. Parkinson's disease: A traffic jam? *Current Biology* 2016; **26**(8): R332-R334.
5. Shahmoradian SH, Lewis AJ, Genoud C, Hench J, Moors TE, Navarro PP, Castano-Diez D, Schweighauser G, Graff-Meyer A, Godie KN, Sutterlin R, Huisman E, Ingrassia A, de Gier Y, Rozemuller AJM, Wang J, De Paepe A, Erny J, Staempfli A, Hoernschemeyer J, Grosserueschkamp F, Niedieker D, El-Mashtoly SF, Quadri M, Van IJcken WFJ, Bonifati V, Gerwert K, Bohrmann B, Frank S, Britschgi M, Stahlberg H, Van de Berg WDJ, Lauer ME. Lewy pathology in Parkinson's disease consists of crowded organelles and lipid membranes. *Nature Neuroscience* 2019; **22**(7): 1099-1109.
6. Prots I, Grosch J, Brazdis R, Simmnacher K, Veber V, Havlicek S, Hannappel C, Krach F, Krumbiegel M, Schuetz O, Reis A, Wrasidlo W, Galasko DR, Groemer TW, Masliah E, Schloetzer-Schrehardt U, Xiang W, Winkler J, Winner B. Alpha-synuclein oligomers induce early axonal dysfunction in human iPSC-based models of synucleinopathies. *Proceedings of the National Academy of Sciences of the United States of America* 2018; **115**(30): 7813-7818.
7. Hollenbeck PJ, Saxton WM. The axonal transport of mitochondria. *Journal of Cell Science* 2005; **118**(23): 5411-5419.
8. Uttara B, Singh AV, Zamboni P, Mahajan RT. Oxidative stress and neurodegenerative diseases: A review of upstream and downstream antioxidant therapeutic options. *Current Neuropharmacology* 2009; **7**(1): 65-74.
9. Misgeld T, Schwarz TL. Mitostasis in neurons: Maintaining mitochondria in an extended cellular architecture. *Neuron* 2017; **96**(3): 651-666.
10. Malka F, Guillery O, Cifuentes-Diaz C, Guillou E, Belenguer P, Lombes A, Rojo M. Separate fusion of outer and inner mitochondrial membranes. *EMBO Reports* 2005; **6**(9): 853-859.

11. Patel PK, Shirihai O, Huang KC. Optimal dynamics for quality control in spatially distributed mitochondrial networks. *PLOS Computational Biology* 2013; **9**(7): e1003108.
12. Twig G, Elorza A, Molina AJA, Mohamed H, Wikstrom JD, Walzer G, Stiles L, Haigh SE, Katz S, Las G, Alroy J, Wu M, Py BF, Yuan J, Deeney JT, Corkey BE, Shirihai OS. Fission and selective fusion govern mitochondrial segregation and elimination by autophagy. *EMBO Journal* 2008; **27**(2): 433-446.
13. Safiulina D, Kaasik A. Energetic and dynamic: How mitochondria meet neuronal energy demands. *PLOS Biology* 2013; **11**(12): e1001755.
14. Cagalinec M, Safiulina D, Liiv M, Liiv J, Choubey V, Wareski P, Veksler V, Kaasik A. Principles of the mitochondrial fusion and fission cycle in neurons. *Journal of Cell Science* 2013; **126**(10): 2187-2197.
15. Ahola S, Langer T, MacVicar T. Mitochondrial proteolysis and metabolic control. *Cold Spring Harbor Perspectives in Biology* 2019; **11**(7): a033936.
16. Melkov A, Abdu U. Regulation of long-distance transport of mitochondria along microtubules. *Cellular and Molecular Life Sciences* 2018; **75**(2): 163-176.
17. Narayanareddy BRJ, Vartiainen S, Hariri N, O'Dowd DK, Gross SP. A biophysical analysis of mitochondrial movement: Differences between transport in neuronal cell bodies versus processes. *Traffic* 2014; **15**(7): 762-771.
18. Ferree AW, Trudeau K, Zik E, Benador IY, Twig G, Gottlieb RA, Shirihai OS. MitoTimer probe reveals the impact of autophagy, fusion, and motility on subcellular distribution of young and old mitochondrial protein and on relative mitochondrial protein age. *Autophagy* 2013; **9**(11): 1887-1896.
19. Hernandez G, Thornton C, Stotland A, Lui D, Sin J, Ramil J, Magee N, Andres A, Quarato G, Carreira RS, Sayen MR, Wolkowicz R, Gottlieb RA. MitoTimer A novel tool for monitoring mitochondrial turnover. *Autophagy* 2013; **9**(11): 1852-1861.
20. Gottlieb RA, Stotland A. MitoTimer: A novel protein for monitoring mitochondrial turnover in the heart. *Journal of Molecular Medicine-JMM* 2015; **93**(3): 271-278.
21. Wilson RJ, Drake JC, Cui D, Zhang M, Perry HM, Kashatus JA, Kusminski CM, Scherer PE, Kashatus DF, Okusa MD, Yan Z. Conditional MitoTimer reporter mice for assessment of mitochondrial structure, oxidative stress, and mitophagy. *Mitochondrion* 2019; **44**: 20-26.
22. Agrawal A, Koslover EF. Optimizing mitochondrial maintenance in extended neuronal projections. *PLOS Computational Biology* 2021; **17**(6): e1009073.
23. Anderson DH. *Compartmental Modeling and Tracer Kinetics.* Springer: Berlin, 1983.

24. Jacquez JA. *Compartmental Analysis in Biology and Medicine.* University of Michigan Press, Ann Arbor, MI: 1985.
25. Jacquez JA, Simon CP. Qualitative theory of compartmental-systems. *SIAM Review* 1993; **35**(1): 43-79.
26. Kuznetsov IA, Kuznetsov AV. Modelling transport and mean age of dense core vesicles in large axonal arbours. *Proceedings of the Royal Society A* 2019; **475**: 20190284.
27. Kuznetsov IA, Kuznetsov AV. How old are dense-core vesicles residing in en passant boutons: Simulation of the mean age of dense-core vesicles in axonal arbours accounting for resident and transiting vesicle populations. *Proceedings of the Royal Society A-Mathematical Physical and Engineering Sciences* 2020; **476**(2241): 20200454.
28. Metzler H, Muller M, Sierra CA. Transit-time and age distributions for nonlinear time-dependent compartmental systems. *Proceedings of the National Academy of Sciences of the United States of America* 2018; **115**(6): 1150-1155.
29. Metzler H, Sierra CA. Linear autonomous compartmental models as continuous-time markov chains: Transit-time and age distributions. *Mathematical Geosciences* 2018; **50**(1): 1-34.
30. Rasmussen M, Hastings A, Smith MJ, Agusto FB, Chen-Charpentier BM, Hoffman FM, Jiang J, Todd-Brown KEO, Wang Y, Wang Y, Luo Y. Transit times and mean ages for nonautonomous and autonomous compartmental systems. *Journal of Mathematical Biology* 2016; **73**(6-7): 1379-1398.
31. Shlevkov E, Schwarz TL, Axonal Mitochondrial Transport. *In: Parkinson's Disease Molecular Mechanisms Underlying Pathology.* Elsevier: Amsterdam, 2017; 113-137.
32. Mandal A, Pinter K, Drerup CM. Analyzing neuronal mitochondria in vivo using fluorescent reporters in zebrafish. *Frontiers in Cell and Developmental Biology* 2018; **6**: 144.
33. Mandal A, Wong HC, Pinter K, Mosqueda N, Beirl A, Lomash RM, Won S, Kindt KS, Drerup CM. Retrograde mitochondrial transport is essential for organelle distribution and health in zebrafish neurons. *Journal of Neuroscience* 2021; **41**(7): 1371-1392.
34. Saxton WM, Hollenbeck PJ. The axonal transport of mitochondria. *Journal of Cell Science* 2012; **125**(9): 2095-2104.
35. Beck JV, Arnold KJ. *Parameter Estimation in Science and Engineering.* Wiley: New York, 1977.
36. Zadeh KS, Montas HJ. A class of exact solutions for biomacromolecule diffusion-reaction in live cells. *Journal of Theoretical Biology* 2010; **264**(3): 914-933.

37. Zi Z. Sensitivity analysis approaches applied to systems biology models. *Iet Systems Biology* 2011; **5**(6): 336-346.
38. Kuznetsov IA, Kuznetsov AV. Investigating sensitivity coefficients characterizing the response of a model of tau protein transport in an axon to model parameters. *Computer Methods in Biomechanics and Biomedical Engineering* 2019; **22**(1): 71-83.
39. Kacser H, Burns J, Fell D. The control of flux. *Biochemical Society Transactions* 1995; **23**(2): 341-366.
40. Anonymous Figure Generated with the Aid of Servier Medical Art, Licensed Under a Creative Common Attribution 3.0 Generic License. http://smart.servier.com.

Figure captions

Fig. 1. (a) A schematic diagram of a neuron with an axon which is assumed to contain *N* energy demand sites. Demand sites are numbered starting with the most proximal (#1) to the most distal (#*N*) [40].

Fig. 2. A diagram of a compartmental model showing transport in the compartments surrounding the demand sites in the terminal. Arrows show mitochondria exchange between the transiting (anterograde and retrograde) states in adjacent demand sites, mitochondria capture into the stationary state and re-release from the stationary state. Mitochondria entering the terminal are assumed to have zero age.

Fig. 3. Steady-state values of the total length of stationary, anterogradely moving, and retrogradely moving mitochondria per unit length of the axon in the compartment by the *i*th demand site.

Fig. 4. Steady-state values of the mean age of stationary, anterogradely moving, and retrogradely moving mitochondria in the compartment by the *i*th demand site.

Fig. 5. Dimensionless sensitivity coefficients of the mean age of mitochondria with respect to parameter k_w in the compartment by the *i*th demand site. Computations were performed with $\Delta k_w = 10^{-3} k_w$. An almost identical result was obtained for $\Delta k_w = 10^{-2} k_w$.

Fig. 6. Dimensionless sensitivity coefficients of the mean age of mitochondria with respect to parameter p_s in the compartment by the *i*th demand site. Computations were performed with $\Delta p_s = 10^{-3} p_s$. An almost identical result was obtained for $\Delta p_s = 10^{-2} p_s$.

Fig. 7. Dimensionless sensitivity coefficients of the mean age of mitochondria with respect to parameter ε in the compartment by the *i*th demand site. Computations were performed with $\Delta\varepsilon = 10^{-3} \varepsilon$. An almost identical result was obtained for $\Delta\varepsilon = 10^{-2} \varepsilon$.

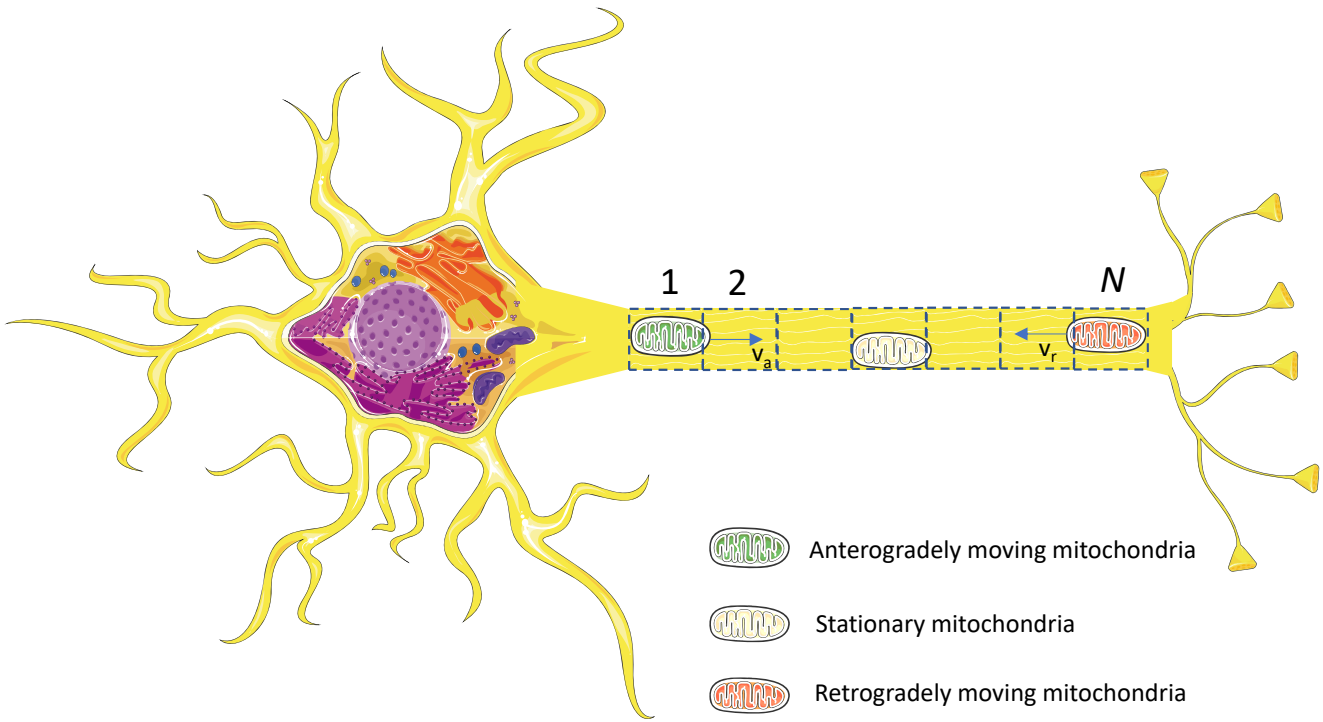
1
2
N
v_a
v_r
Anterogradely moving mitochondria
Stationary mitochondria
Retrogradely moving mitochondria

Figure 1

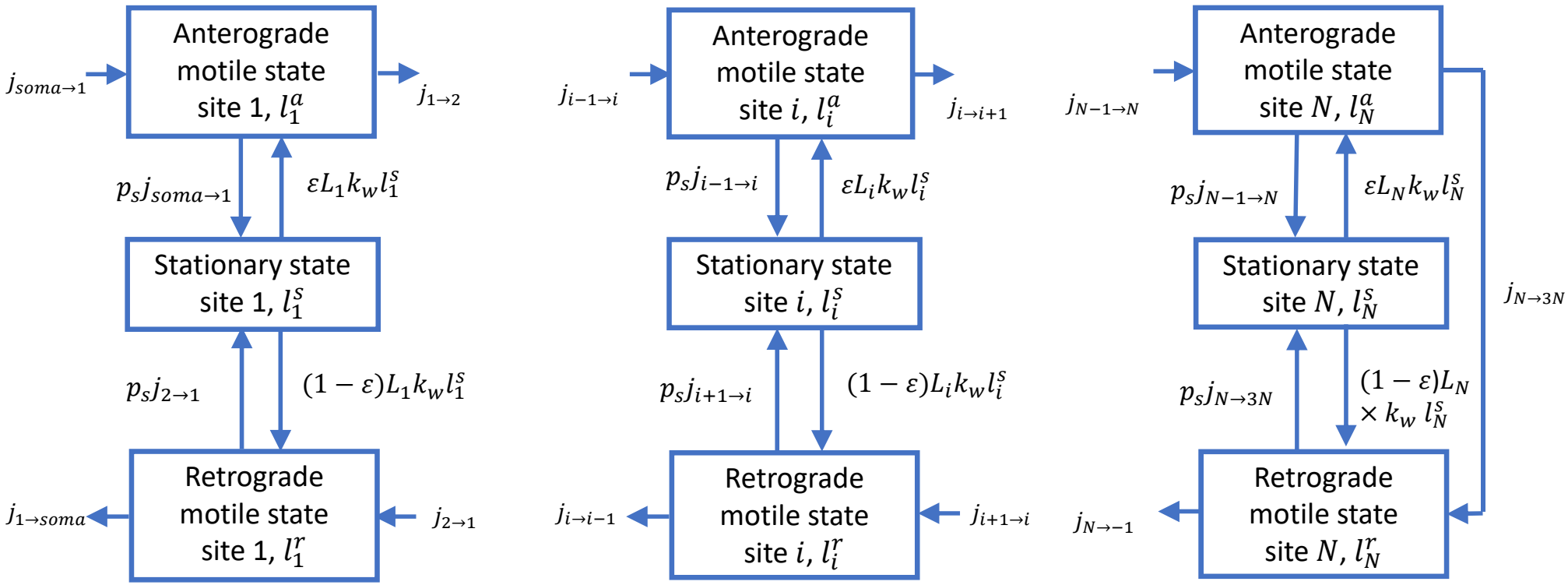
Anterograde motile state site 1, l_1^a
$j_{soma\to1}$
$j_{1\to2}$
$p_s j_{soma\to1}$
$\varepsilon L_1 k_w l_1^s$
Stationary state site 1, l_1^s
$p_s j_{2\to1}$
$(1-\varepsilon)L_1 k_w l_1^s$
Retrograde motile state site 1, l_1^r
$j_{1\to soma}$
$j_{2\to1}$
Anterograde motile state site i, l_i^a
$j_{i-1\to i}$
$j_{i\to i+1}$
$p_s j_{i-1\to i}$
$\varepsilon L_i k_w l_i^s$
Stationary state site i, l_i^s
$p_s j_{i+1\to i}$
$(1-\varepsilon)L_i k_w l_i^s$
Retrograde motile state site i, l_i^r
$j_{i\to i-1}$
$j_{i+1\to i}$
Anterograde motile state site N, l_N^a
$j_{N-1\to N}$
$p_s j_{N-1\to N}$
$\varepsilon L_N k_w l_N^s$
Stationary state site N, l_N^s
$j_{N\to 3N}$
$p_s j_{N\to 3N}$
$(1-\varepsilon)L_N \times k_w\ l_N^s$
Retrograde motile state site N, l_N^r
$j_{N\to -1}$

Figure 2

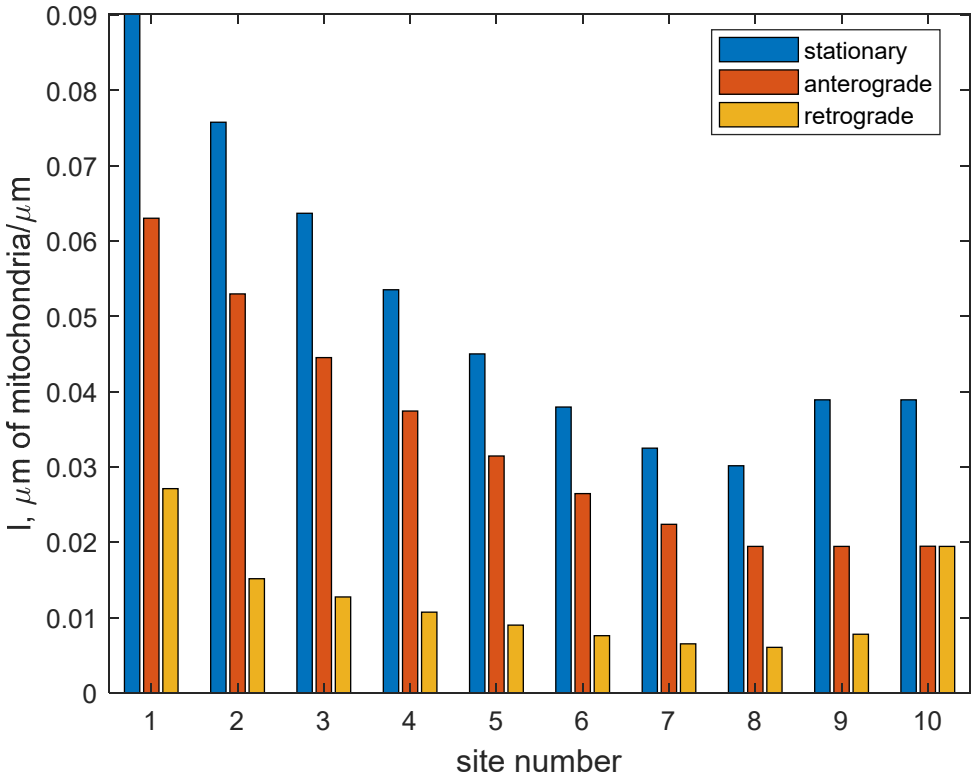
0.09
0.08
0.07
0.06
0.05
0.04
0.03
0.02
0.01
0
l, μm of mitochondria/μm
1
2
3
4
5
6
7
8
9
10
site number
stationary
anterograde
retrograde

Figure 3

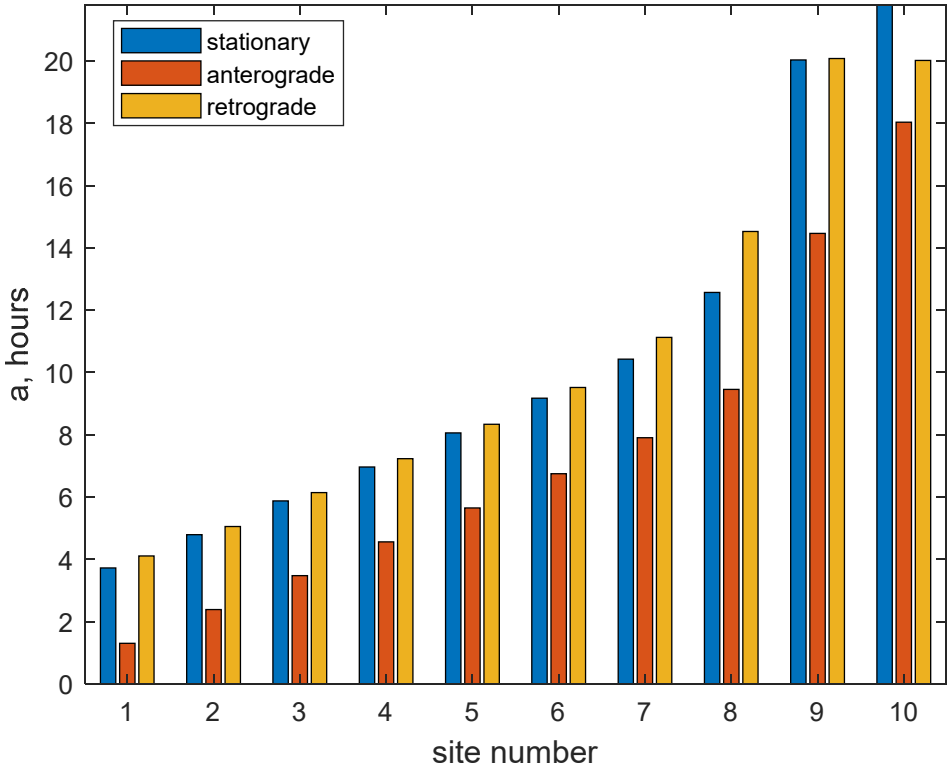
stationary
anterograde
retrograde
a, hours
site number
0
2
4
6
8
10
12
14
16
18
20
1
2
3
4
5
6
7
8
9
10

Figure 4

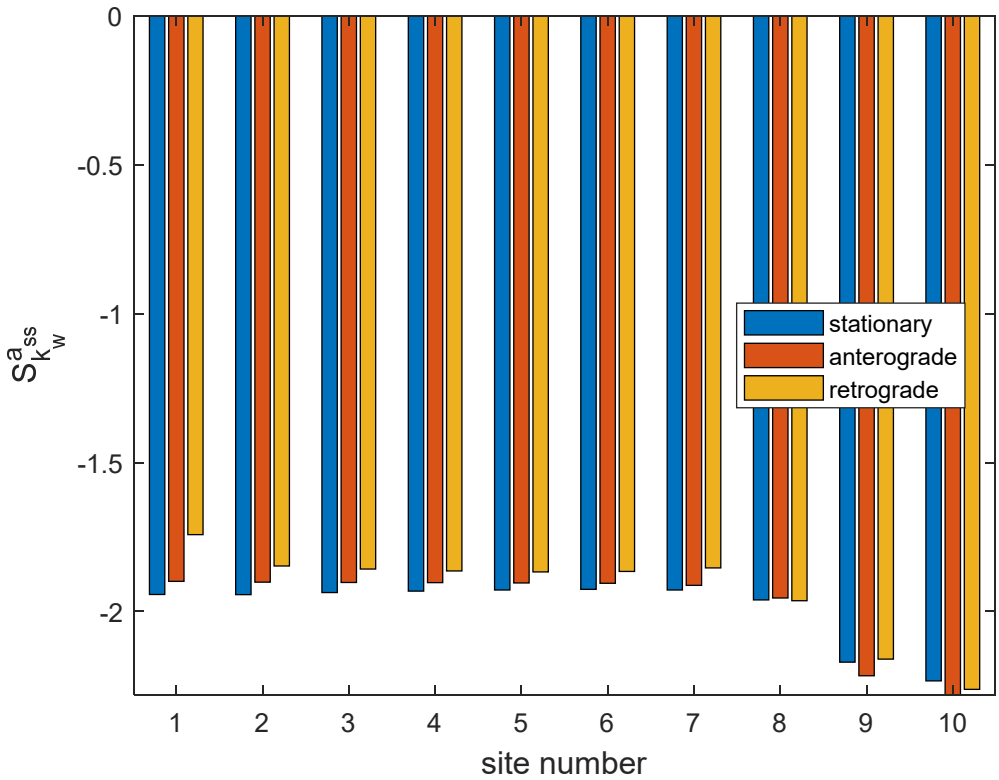
0
-0.5
-1
-1.5
-2
$S^{a}_{k^{ss}_{w}}$
stationary
anterograde
retrograde
1
2
3
4
5
6
7
8
9
10
site number

Figure 5

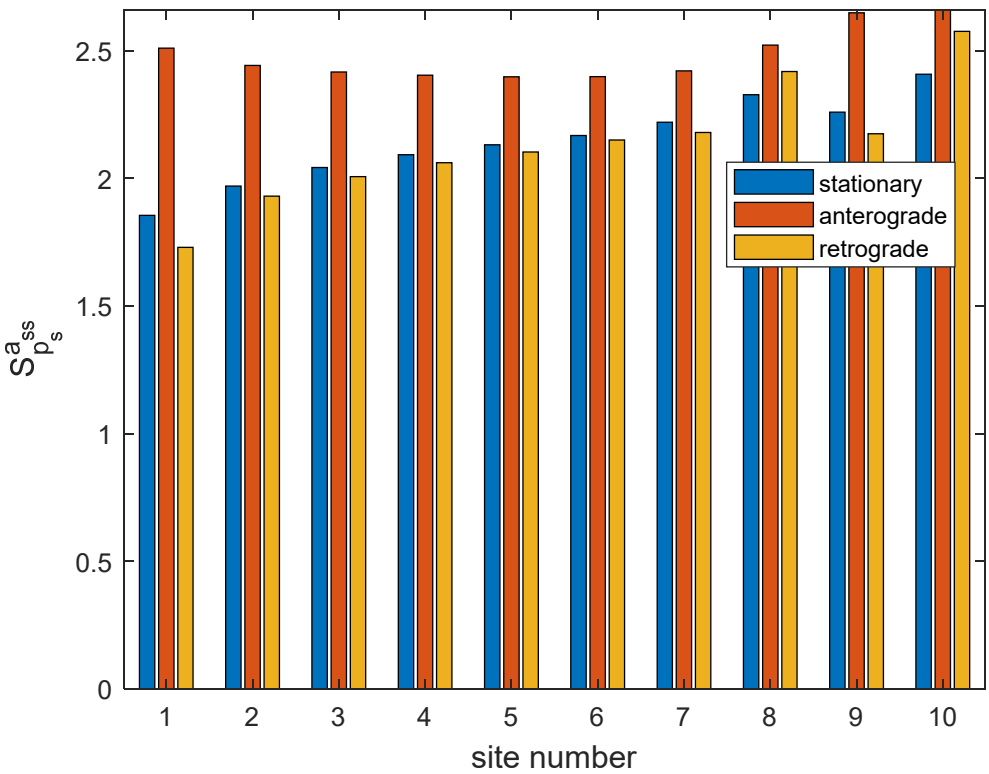
2.5
2
1.5
1
0.5
0
$S^{a}_{p^{ss}_{s}}$
1
2
3
4
5
6
7
8
9
10
site number
stationary
anterograde
retrograde

Figure 6

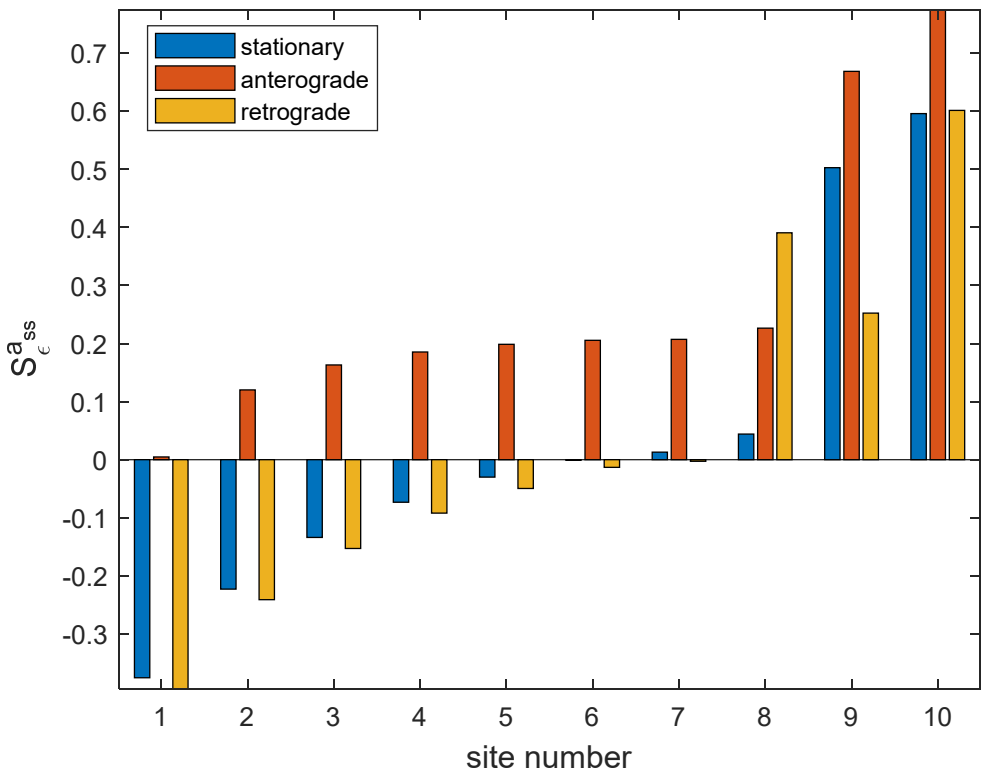
stationary
anterograde
retrograde
0.7
0.6
0.5
0.4
0.3
0.2
0.1
0
-0.1
-0.2
-0.3
$S^a_{\epsilon^{ss}}$
1
2
3
4
5
6
7
8
9
10
site number

Figure 7